

Simulation for the oblique impact of a lattice system

Hiroto KUNINAKA ^{*} and Hisao HAYAKAWA [†]

GSSES, Kyoto University, Sakyo-ku, Kyoto 606-8502

(Dated: November 5, 2018)

Abstract

The oblique collision between an elastic disk and an elastic wall is numerically studied. We investigate the dependency of the tangential coefficient of restitution on the incident angle of impact. From the results of simulation, our model reproduces experimental results and can be explained by a phenomenological theory of the oblique impact.

^{*} E-mail address: kuninaka@yuragi.jinkan.kyoto-u.ac.jp

[†] E-mail address: hisao@yuragi.jinkan.kyoto-u.ac.jp

I. INTRODUCTION

Collisions are common phenomena in nature. In macroscopic scales, we often see collisions of balls in sports such as the baseball and the billiard. In such collisions, the initial kinetic energy of material dissipates into internal degrees of freedom. A part of total energy is distributed into the translational motion and the rotational motion, while the other part is dissipated as elastic vibration, sound emission, heat, etc. As a result, collisions of macroscopic material are always inelastic.

Inelastic collisions play important roles in granular materials[1, 2]. Characteristic behaviors of granular material come from inelastic collisions among particles. The *Distinct Element Method* (DEM) is a standard method of simulation for the granular materials[3]. DEM contains some phenomenological parameters such as the Coulomb's coefficient of friction, dashpots, and so on. Nobody can determine such the viscoelastic parameter from the first principle. Even the determination of the simplest parameter, the coefficient of restitution (COR), is difficult.

COR is a familiar parameter which is introduced in text books of the elementary physics. The normal COR is defined by the ratio of the normal components of the collision velocity before and after collision. Figure 1 is the schematic figure that a sphere is colliding with a stationary wall with initial velocity of its center of mass, \mathbf{v} . The prime denotes post-colliding quantities. The coefficient of normal restitution e is defined by

$$\mathbf{v}'_{\mathbf{c}} \cdot \mathbf{n} = -e\mathbf{v}_{\mathbf{c}} \cdot \mathbf{n}, \quad (1)$$

where $\mathbf{v}_{\mathbf{c}}$ and $\mathbf{v}'_{\mathbf{c}}$ are respectively the velocity of the contact point before and after the collision. e is assumed to be $0 \leq e \leq 1$. Historically, COR was first introduced by Newton[4]. Though many text books of elementary physics state that e is a material constant, many experiments and simulations show that e decreases as the impact velocity increases[5, 6, 8, 9, 10, 11?] except for the idealized situation of a collision between two rods, in which e may be determined by the ratio of length of the colliding rods[12, 13, 14, 15, 16]. Recently, Louge and Adams have reported that e can exceeds unity in an oblique impact[17]. The mechanism of the exotic behavior has not been clarified yet. Thus, study of collisions is not matured and has room for development though the subject itself is familiar even for high school students.

In addition to e , the tangential COR β is also important to characterize oblique impacts, where β is defined as

$$\mathbf{v}'_c \cdot \mathbf{t} = -\beta \mathbf{v}_c \cdot \mathbf{t}, \quad (2)$$

where \mathbf{v}'_c and \mathbf{t} are the post-collisional velocity at the contact point after collision and the unit tangential vector, respectively. β is a function of the angle of incidence γ which is defined as $\gamma = \arctan(v_t/v_n)$ with $v_n = \mathbf{v}_c \cdot \mathbf{n}$ and $v_t = \mathbf{v}_c \cdot \mathbf{t}$ and is believed that possible values of β lie between -1 and 1 [18, 19, 20, 21, 22].

The aim of our study is to investigate β in detail from numerical simulation. We study the relation between β and the angle of incidence in oblique collision in this paper. The organization of this paper is as follows. In §2, we will review the current status of the researches about inelastic collisions. In §3, we introduce our numerical model and setup of the simulation. Section 4 is the main part of this paper where we summarize the results of our simulation and compare them with the theoretical outcome. Section 5 is devoted to the discussion of our results. The last section is the conclusion remarks. In Appendix A, we will give a description of the theory of the oblique impact. In Appendix B, the derivation of Poisson's ratio of the square lattice system will be introduced.

II. REVIEW

In this section, we review current status of the study of inelastic collision. At the end of the 19th century, it became clear experimentally that COR depends on the relative velocity of the colliding materials [23]. In the normal collision of spheres, it is believed that COR obeys $1 - e \propto v^{1/5}$ when impact velocity v is low enough while $e \propto v^{-1/4}$ when v exceeds the critical value of plastic deformations. In fact, Sondergaard *et al.* [8] performed an impact experiment of ball bearings and glass spheres on lucite or aluminum plates and confirmed the dependency on the impact velocity as $e \propto v^{-1/4}$ in the high speed impact. Johnson explained this dependency using the dimensional analysis [6]. His analysis was consistent with the experimental data. Kuwabara and Kono [11] investigated COR for low speed impact and derived the theoretical expression $1 - e \propto v^{1/5}$ which is consistent with their experimental results. Recently, some papers about quasi-static theory are published which are consistent with Kuwabara and Kono [24, 25, 26, 27].

On the other hand, Gerl and Zippelius performed simulation of a two-dimensional collision

of an elastic disk with an elastic wall[28]. The present authors performed two-dimensional simulations and confirmed that elastic models including that of Gerl and Zippelius is not appropriate to characterize the quasi-static region[29, 30, 31].

To characterize the oblique collision, Walton introduced three parameters: the coefficient of normal restitution e , the coefficient of Coulomb's friction μ_0 , and the maximum value of the coefficient of tangential restitution β_0 [18]. Experiments have supported that his characterization adequately capture the essence of binary collision of spheres or collision of a sphere on a flat plate[19, 20, 21, 22]. Walton derives

$$\beta \simeq \begin{cases} -1 + \mu_0(1 + e) \cot \gamma \left(1 + \frac{mR^2}{I}\right) & (\gamma \geq \gamma_0) \\ \beta_0 & (\gamma \leq \gamma_0), \end{cases} \quad (3)$$

where γ_0 is the critical angle, and m , R , and I are mass, radius and moment of inertia of spheres respectively.[18] Experimental results are consistent with eq.(3)[19, 20, 21, 22]. Meanwhile, Maw *et al.* extended the Hertz theory of impact[32, 33, 34, 35] and established the theory of the oblique impact to be consistent with their experimental results[36, 37]. The theory by Maw *et al.* has several advantages: (i) The physical mechanism is included in their theory but not in Walton's argument. (ii) Anomalous behavior near $\gamma = 0$ can be described in their theory. The disadvantage of their argument is that we cannot summarize the result of theory in a concise form as in eq.(3). Thus, we still use both Walton's expression and the theory by Maw *et al.*. The details of the theory by Maw *et al.* and its application to our results is summarized in Appendix A.

III. OUR MODELS

In this section, let us introduce our numerical model. Our numerical model consists of an elastic disk and an elastic wall (Fig. 2). Both of them are composed of randomly distributed 1600 mass points. We use the Delaunay triangulation algorithm to connect all mass points with nonlinear springs[38]. The spring interaction between connected mass points is described as

$$V(x) = \frac{1}{2}k_a x^2 + \frac{1}{4}k_b x^4, \quad (4)$$

where x is a stretch from the natural length of spring, and k_a and k_b are the spring constants. In most of simulations, we adopt $k_a = 1.0 \times mc^2/R^2$ and $k_b = 1.0 \times 10^{-3}mc^2/R^4$, respectively.

The width of the wall is 4 times as long as the diameter of the disk while the height of the wall is same as the diameter of the disk. Two sides of the wall are fixed.

The interaction between the disk and the wall during a collision is introduced as follows. Figure 3 is the schematic figure of the interaction of surface mass points of the disk and the wall. When the distance l between the lower edge of the disk and the surface of the wall becomes less than the cutoff length which is the mean value of natural lengths of all springs, the surface particles of the disk feel the repulsive force, $\mathbf{F}(l) = aV_0 \exp(-al)\mathbf{n}$, where a is $300/R$, V_0 is $amc^2R/2$, m is the mass of the particle, R is the radius of the disk, $c = \sqrt{E/\rho}$, E is Young's modulus, and ρ is the density, \mathbf{n} is the normal unit vector to the surface. The reaction forces applied to the two points of the surface of the wall (point 1 and 2) are decided by the balance of the torques as $\mathbf{F}_1(l) = -F(l)\mathbf{n}/(1+l_1/l_2)$ and $\mathbf{F}_2(l) = -F(l)\mathbf{n}/(1+l_2/l_1)$, where $l_i (i = 1, 2)$ is the distance between the point p and the point i (see Fig. 3).

In this model, roughness of the surfaces is important to make the disk rotate after collisions. To make roughness, at first, we generate normal random numbers whose average value is 0 and then make the initial position of particles on surfaces of both the disk and the wall deviate with them. We choose the standard deviation of the normal random numbers δ as $\delta = 3 \times 10^{-2}R$, where R is the radius of the disk. All of the data presented here are obtained from the average of 100 samples in random numbers.

For random lattice model, it is impossible to determine Poisson's ratio ν and Young's modulus E theoretically. When we determine Poisson's ratio ν and Young's modulus E of this model, we add the viscous force term in equation of motion which is proportional to the relative velocity of two connected mass points. By stretching the band of random lattice and calculating the ratio of the strains in the vertical and horizontal directions to the force and the ratio of the strain to the force when the vibration stops, we can obtain Poisson's ratio and Young's modulus. Figure 4(a) and 4(b) are snap shots of the bands of random lattice made of 348 mass points before and after adding the force $F = 3.0 \times 10^2 mc^2/R$, respectively. We change the force from $2.0 \times 10^2 mc^2/R$ to $3.0 \times 10^2 mc^2/R$ and average 10 samples of results to obtain $\nu = (7.50 \pm 0.11) \times 10^{-2}$ and $E = (9.54 \pm 0.231) \times 10^3 mc^2/R^2$, respectively.

For comparison, we introduce other two lattice models for elastic disks: triangular lattice and square lattice disk(Fig.5). To investigate the effect of the structure of the disk, the wall is same as random lattice model. In order to remove anisotropies of lattice structure, we

put an exterior layer which is same as random lattice disk around the disk and bind all of them using the Delaunay triangulation algorithm. The triangular lattice disk is made by replacing the internal structure of the random lattice disk with the triangular lattice. Total number of mass points is same as that of random disk. Poisson's ratio and Young's modulus of the triangular lattice can be calculated theoretically as $1/3$ and $2k_a/\sqrt{3}$ in the continuum limit respectively[39]. The square lattice disk is made by replacing the internal structure of the random lattice disk with the square lattice and connecting all the mass points by the Delaunay triangulation algorithm. We introduce two spring constants: $k_a = k_1$ for nearest neighbor interaction and $k_a = k_2$ for next-nearest neighbor interaction. In the continuum limit, Young's modulus E [40] and Poisson's ratio ν (see Appendix B) of the square lattice are expressed as

$$\frac{1}{E} = \frac{k_1 + k_2}{k_1(k_1 + 2k_2)} + \frac{k_1 - 2k_2}{k_1 k_2} n_x^2 n_y^2, \quad (5)$$

$$\nu = \frac{k_2^2 + (k_1^2 - 4k_2^2) n_x^2 n_y^2}{k_2(k_1 + k_2) + (k_1^2 - 4k_2^2) n_x^2 n_y^2}, \quad (6)$$

where n_x and n_y are the unit normal vectors horizontal and vertical to the collisional plane. The derivation of eqs.(5) and (6) is presented in Appendix B. To recover the orientational symmetry and introduce roughness on the surface of disks, we introduce one-layer random lattice on the surface of the disks.

We scale the equation of motion for each particle using the radius of the disk R as the scale of length and the velocity of elastic wave $c = \sqrt{E/\rho}$ as the scaling unit of velocity. As the numerical scheme of the integration, we use the fourth order symplectic numerical method with the time step $\Delta t \simeq 10^{-3} R/c$.

IV. RESULTS

In this section, we explain the results of our simulation. The angle of incidence γ is ranged from 5.7° to 80.5° while the normal component of velocity is fixed as $0.1c$. The colliding disk has no internal vibration and rotation at release time. In order to eliminate the effect of the initial configuration of mass points, we prepare 100 samples of disk as the initial condition by using 100 sets of normal random numbers and average data of all samples.

Figure 6 shows the relation between $\cot \gamma$ and the coefficient of tangential restitution β . In this figure, cross points are the result of the impact between random lattice disk and wall,

and broken lines are eq.(3). In eq.(3) we use the value $e = 0.8$ which is the approximate mean value of e in the range $2.5 \leq \cot \gamma \leq 6$ in Fig.7. The result of simulation shows that β_0 is 0.56 and μ_0 is 0.18 which are close to the values observed in experiments of three dimensional impacts[19, 20]. Thus, we reproduce experimental tendencies of the oblique collision with the random lattice model[19, 20]. Stars are the results of random lattice disk without roughness on the surface, in which β is close to -1 . From this result, one can see that roughness on the surface is important for the rotation of the disk after collision. Plus points in Fig.6 are the result of the triangular lattice model where the orientation of initial disks is same as that in Fig.5(a). In this model, β takes negative values in all range of the angle of incidence. This means that the disk made of triangular lattice is easy to slip on the surface. In addition, the result strongly depends on the initial orientation of the disk. Thus, the model of triangular lattice is inadequate to reproduce the tendency of experimental data.

Figure 7 shows the relation between $\cot \gamma$ and e . Although e is expected to be a constant because the normal velocity of the disk is fixed, COR depends on γ . In particular, for small $\cot \gamma$, e decreases as $\cot \gamma$ decreases. We will discuss this behavior in the later discussion.

Here, we compare our result with the theory of Maw *et al.*[7, 36, 37] which was consistent with experimental data[20, 21, 22, 36, 37]. According to their theory, all the region of the angle of incidence can be divided into three regimes. For each regime, β can be expressed as

1. $1/\mu\eta^2 < \cot \gamma$:

$$\beta = -\cos \omega t_1 - \mu \frac{\beta_x}{\beta_z} e \left[1 + \cos \left(\frac{\Omega t_1}{e} + \frac{\pi}{2} (1 - e^{-1}) \right) \right] \cot \gamma, \quad (7)$$

2. $\beta_x/\beta_z\mu(1+e) < \cot \gamma < 1/\mu\eta^2$:

$$\begin{aligned} \beta = & -\cos \omega(t_3 - t_2) - \mu \frac{\beta_x}{\beta_z} [\cos \omega(t_3 - t_2) - \cos \Omega t_2 \cos \omega(t_3 - t_2) \\ & + \frac{\Omega}{\omega} \sin \Omega t_2 \sin \omega(t_3 - t_2) + e + \cos \Omega t_3] \cot \gamma, \end{aligned} \quad (8)$$

3. $\cot \gamma < \beta_x/\beta_z\mu(1+e)$:

$$\beta = -1 + \mu \frac{\beta_x}{\beta_z} (1 + e) \cot \gamma, \quad (9)$$

where μ is the coefficient of friction, η is the constant dependent on Poisson's ratio defined in eq.(A5), β_x and β_z are constants calculated from mass, radius, and radii of gyration of

material as $\beta_x = 3.02$ and $\beta_z = 1$ as shown in eq.(A2). Ω and ω are respectively $\pi/2t_c$ and $(\pi/2\eta t_c)\sqrt{\beta_x/\beta_z}$, where t_c is a duration of a collision. t_1 determined by eq.(A10) is the transition time from initial stick motion to slip motion. t_3 determined by eqs.(A21) and (A20) is the transition time from slip motion to stick motion. By calculating β at each value of $\cot \gamma$ and interpolating them with cubic spline interpolation method, we can draw the theoretical curve.

We compare the result of simulation of the oblique impact using the random lattice model with the theoretical curve(Fig.8). Here we used $\eta = 1.015$, $e = 0.8$ which is an average value of COR in Fig.7, and $\mu = 0.18$ which is decided by comparing the slope in the small $\cot \gamma$ region with eq.(3). It is found that the result of random lattice model is consistent with the theory especially in small $\cot \gamma$ region. In the intermediate region, the agreement of the data with the theory is worse than that of other regions. This tendency can be seen in some experimental results [20, 22, 37].

Theoretical result by Maw *et al.* suggests that Poisson's ratio is not a crucial parameter to determine β , while Poisson's ratio of the triangular lattice is much larger than that of the random lattice. To confirm that anomalous behavior of the triangular lattice comes from the specific lattice structure we simulate the collision by using the square lattice model. By changing the value of spring constants of square lattice disk and controlling Poisson's ratio, we investigate the dependency of β_0 on Poisson's ratio. β_0 are 0.49 and 0.51 when $\nu = 0.1$ and $\nu = 0.3$, respectively. From these results, we confirm that Poisson's ratio is not a crucial parameter for β_0 .

V. DISCUSSIONS

Here, we discuss the results of our simulation. We change the number of mass points of random lattice model and investigate the dependency on the system size. As the number of mass points becomes larger, there is a tendency for a graph to be flattened in the region of large $\cot \gamma$. It can be seen as follows. When the model is composed of many mass points, irregularity of the surface of the random lattice diminishes as the size of the disk increases. As a result, β_0 can take the stable value in the large $\cot \gamma$. When the number of mass points is larger than 1600, all the mass points in the rectangle cannot be connected by the Delaunay triangulation algorithm[38]. Hence, our results are restricted to the case with the 1600 mass

points as the maximum value.

We also investigate the influence of roughness of the surface. When the standard deviation δ takes $2.15 \times 10^{-2}R$, β increases monotonously as $\cot \gamma$ increases. When δ takes $3.0 \times 10^{-3}R$, β approaches the stable maximum value $\beta_0 = 0.56$. For larger δ , the surface of the rectangle is easy to collapse when the collision occurs. As for μ_0 , μ_0 takes 0.14 when δ is $2.15 \times 10^{-2}R$ while μ_0 takes 0.18 when δ is $3.0 \times 10^{-2}R$. It can be seen that roughness of the surface make the value of μ_0 increase.

Random lattice model can reproduce experimental tendency in β_0 and μ_0 with roughness on the surface. However, the random lattice model cannot reproduce the tendency that β decreases from the maximum value β_0 in the large $\cot \gamma$ [19]. Other mechanisms like sticking or plastic deformation on the surface may be important in the large γ region.

From Fig.6, the triangular lattice disk seems to be inadequate to reproduce experimental tendency. In triangular lattice, the shape of the disk is much more like a polygon than a circle. It may be that polygonal property of the structure causes the slip motion of the disk.

The decrease of e in the small $\cot \gamma$ in Fig.7 can be understood as follows. In our situation, normal component of initial velocity is fixed to $0.1c$. Thus, the initial kinetic energy of the disk becomes larger in the small $\cot \gamma$. As a result, the surface of the wall cannot seize the disk so that the initial kinetic energy is easy to propagate in the horizontal direction to the surface of the wall.

In the last section we investigated the dependency on Poisson's ratio with the aid of the square lattice model. In contrast, we change the value of k_a of the triangular lattice disk from $1.0 \times mc^2/R^2$ to $1.0 \times 10^2 mc^2/R^2$ to investigate the dependency on Young's modulus. Although Young's modulus increases by 100-fold, the triangular lattice disk remains slippery on the surface. From this fact, it can be seen that Young's modulus as well as Poisson's ratio are not crucial. In addition, we change the value of k_b of triangular lattice disk from $1.0 \times 10^{-3} mc^2/R^4$ to $1.0 \times 10^{-1} mc^2/R^4$ and investigate the effect of the nonlinear term of eq.(4). The change of k_b also does not affect the results of triangular lattice disk. It can be seen that the nonlinear term of eq.(4) only strengthen the surface of the model and does not make the triangular lattice disk rotate after collision. In the triangular lattice disk, the polygonal property of the surface of triangular lattice may affect the results.

Finally, we refer to the connection between μ_0 in eq.(3) and μ in eq.(9). In Fig.8, the value of μ is same as μ_0 estimated from the slope in the range $0 \leq \cot \gamma \leq 2$ in Fig.6.

Comparing eq.(3) with eq.(9), we can derive the relation between μ_0 and μ as

$$\mu \frac{\beta_x}{\beta_z} = \mu_0 \left(1 + \frac{mR^2}{I} \right). \quad (10)$$

In the two dimensional binary collision of disks, $1 + mR^2/I$ can be calculated as 3 explicitly. Meanwhile, β_x/β_z in our system can be calculated as 3.02. Thus, μ and μ_0 are in our case almost identical.

VI. CONCLUSION REMARKS

In this paper, we demonstrate the 2-dimensional simulation of the oblique impact. Our random lattice model produces the same tendency as experimental data qualitatively while triangular lattice model can not produce the positive value of β_0 . For normal COR, e depends on the initial angle of incidence and decreases in the large γ when the normal component of initial velocity is fixed. For β , we compare our results with Maw's theory of the oblique impact. Our result is consistent with their theory especially in the large and small region of $\cot \gamma$.

We appreciate Y. Tanaka, Y. Hayakawa and S. Nagahiro for fruitful discussion. We also thank M. Doi and S. Takesue for their valuable comments. Parts of numerical computation in this work were carried out at the Yukawa Institute Computer Facility. This work is partially supported by Hosokawa Powder Technology Foundation and Inamori Foundation.

-
- [1] L. P. Kadanoff: Rev. Mod. Phys. **71** (1999) 435 .
 - [2] P. G. de Gennes: Rev. Mod. Phys. **71** (1999) S374 and references therein.
 - [3] P. A. Cundall, O. D. L. Strack: Géotechnique **29** (1979) 47 .
 - [4] I. Newton: Philosophiae naturalis Principia mathematica (W. Dawson and Sons, London, 1962). The original one has been published in 1687.
 - [5] W. Goldsmith: *Impact: The Theory and Physical Behavior of Colliding Solids* (Edward Arnold Publ., London, 1960).
 - [6] K. L. Johnson: *Contact Mechanics* (Cambridge University Press, Cambridge, 1985).
 - [7] W. J. Stronge: *Impact Mechanics* (Cambridge Univ. Press, 2000).

- [8] R. Sondergaard, K. Chaney, and C. E. Brennen: ASME J. Appl. Mech. **57** (1990) 694 .
- [9] F. G. Bridges, A. Hatzes, and D.N.C. Lin: Nature **309** (1984) 333.
- [10] K. D. Supulver, F. G. Bridges, and D. N. C. Lin: ICARUS **113** (1995) 188.
- [11] G. Kuwabara and K. Kono: Jpn. J. Appl. Phys. **26** (1987) 1230.
- [12] G. Giese and A. Zippelius: Phys. Rev. E **54** (1996) 4828.
- [13] T. Aspelmeier, G. Giese and A. Zippelius: Phys. Rev. E **57** (1998) 857.
- [14] A. G. Basile and R. S. Dumont: Phys. Rev. E **61** (2000) 2015 .
- [15] M. Sugiyama and N. Sasaki: J. Phys. Soc. of Jpn. **68** (1999) 1859.
- [16] S. Nagahiro and Y. Hayakawa: cond-mat/0210374.
- [17] M. Y. Louge and M. E. Adams: Phys. Rev. E **65** (2002) 021303.
- [18] O. R. Walton and R. L. Braun: J. Rheol. **30** (1986) 949.
- [19] L. Labous, A. D. Rosato, and R. N. Dave: Phys. Rev. E **56** (1997) 5717 .
- [20] S. F. Foerster, M. Y. Louge, H. Chang, and K. Allia: Phys. Fluids **6** (1994) 1108.
- [21] A. Lorentz, C. Tuozzolo, and M. Y. Louge: Exp. Mech. **37** (1997) 292.
- [22] D. A. Gorham, A. H. Kharaz: Powder Technology **112** (2000) 193.
- [23] J. H. Vincent: Proc. Cambridge, Phil. Soc. **10** (1900) 332.
- [24] W. A. Morgado and I. Oppenheim: Phys. Rev. E **55** (1997) 1940.
- [25] N. Brilliantov, F. Spahn, J.-M. Hertzsch and T. Pöschel: Phys. Rev. E **53** (1996) 5382.
- [26] T. Schwager and T. Pöschel: Phys. Rev. E **57**, 650 (1998).
- [27] R. Ramírez, T. Pöschel, N. Brilliantov and T. Schwager, Phys. Rev. E **60**, 4465 (1999).
- [28] F. Gerl and A. Zippelius: Phys. Rev. E **59** (1999) 2361 .
- [29] H. Kuninaka and H. Hayakawa: J. Phys. Soc. Jpn. **70** (2001) 2220.
- [30] H. Kuninaka and H. Hayakawa: *Proc. Traffic and Granular Flow 2001* (to be published).
- [31] H. Hayakawa and H. Kuninaka: Chem. Eng. Sci. **57** (2002) 239.
- [32] L. D. Landau and E. M. Lifshitz: *Theory of Elasticity (2nd English ed.)* (Pergamon, New York, 1960).
- [33] A. E. H. Love: *A Treatise on the Mathematical Theory of Elasticity* (Cambridge Univ. Press, 1927).
- [34] D. A. Hills, D. Nowell, and A. Sackfield: *Mechanics of elastic contacts* (Oxford: Butterworth-Heinemann, 1993).
- [35] H. Hertz: J. Reine Angew. Math. **92** (1882) 156.

- [36] N. Maw, J. R. Barber, and J. N. Fawcett: *Wear* **38** (1976) 101.
- [37] N. Maw, J. R. Barber, and J. N. Fawcett: *ASME J. Lub. Tech* **103** (1981) 74.
- [38] K. Sugihara: *Data Kouzou To Algorithm* (Data Structure and Algorithms)(Kyoritsu, Japan, 2001), p. 113 [in Japanese].
- [39] W. G. Hoover: *Computational Statistical Mechanics* (Elsevier Science Publishers B. V., Amsterdam, 1991).
- [40] Y. Hayakawa: *Phys. Rev. E* **49** (1994) R1804.
- [41] R. P. Feynman, R. B. Leighton, and M. Sands: *Lectures on Physics Vol. 2* (Addison-Wesley, Reading, MA, 1964).

- Fig.1 : The schematic figure of a collision of a disk with a wall.
- Fig.2 : The elastic disk and wall consisted of random lattice system.
- Fig.3 : Interaction between surface particles of the disk and the wall.
- Fig.4 : The bands of random lattice (a) before and (b) after stretch.
- Fig.5 : The schematic figures of (a) triangular lattice disk and (b) square lattice disk.
- Fig.6 : The relation between cotangent of angle of incidence γ and β . Cross points are the results of the random lattice disk. Stars are the result when the random disk has no roughness. Plus points are the results of the triangular lattice disk. Dashed and dot-dash lines are eq.(3).
- Fig.7 : The relation between cotangent of angle of incidence γ and COR e .
- Fig.8 : The relation between $\cot \gamma$ and β . Cross points are the numerical results of the random lattice model. Solid line is the theoretical curve.
- Fig.9 : The schematic figure of the disk and the wall. A cross in a circle represents a center of mass of each body.

APPENDIX A: THE THEORETICAL DESCRIPTION OF THE OBLIQUE IMPACT

Here, we review and rewrite a theory of the oblique impact[7, 36, 37] for our investigation. Let a disk with the radius R and a rectangle with the height $2R$ and the width $8R$ be in contact each other as depicted in Fig.(9). They have masses M and M' and their radii of gyration $\hat{k}_r = R/\sqrt{2}$ and $\hat{k}'_r = R\sqrt{17/3}$ around their centers of mass, respectively. The prime denotes parameters for the rectangle. The position of the contact point C is denoted as $(r_x, r_z) = (0, -R)$ or $(r'_x, r'_z) = (0, R)$ which are measured from the centers of mass of each colliding body. Here, v_i and u_i ($i = x, z$) are relative velocity and relative displacement at the contact point, respectively. We assume that both normal and tangential elements of the compliance are proportional to the compression. We also introduce the normal stiffness during compression κ , and the tangential stiffness during compression κ/η^2 for the disk. The equation of motion of the displacements, thus, becomes

$$\begin{pmatrix} \ddot{u}_x \\ \ddot{u}_z \end{pmatrix} = -m^{-1}\kappa \begin{bmatrix} \beta_x\eta^{-2} & 0 \\ 0 & \beta_z \end{bmatrix} \begin{pmatrix} u_x \\ u_z \end{pmatrix}, \quad (\text{A1})$$

where $\ddot{u}_x = d^2u_x/dt^2$, and

$$\beta_x = 1 + \frac{mr_z^2}{M\hat{k}_r^2} + \frac{mr_z'^2}{M'\hat{k}'_r{}^2}, \quad \beta_z = 1 + \frac{mr_x^2}{M\hat{k}_r^2} + \frac{mr_x'^2}{M'\hat{k}'_r{}^2}, \quad (\text{A2})$$

where $1/m = 1/M + 1/M'$. In our situation, β_x and β_z can be calculated as $\beta_x \simeq 3.02$ and $\beta_z = 1$.

Equation of motion (A1) has two characteristic frequencies, Ω and ω , which are expressed as

$$\Omega \equiv \sqrt{\frac{\beta_z\kappa}{m}}, \quad \omega \equiv \sqrt{\frac{\beta_x\kappa}{\eta^2m}} = \frac{1}{\eta}\sqrt{\frac{\beta_x}{\beta_z}}\Omega \quad (\text{A3})$$

in the normal and tangential direction to the wall, respectively. One can also express them using t_c , which is the moment when the normal velocity of compression becomes 0 ($\dot{u}_z(t_c) = 0$), as $\Omega = \pi/2t_c$ and $\omega = (\pi/2\eta t_c)\sqrt{\beta_x/\beta_z}$. According to Johnson[6], stiffnesses in the normal and tangential direction, κ and κ/η^2 , can be expressed using Young's modulus E , the radius of punch a , and Poisson's ratio ν as

$$\kappa = \frac{Ea}{1-\nu^2}, \quad \kappa/\eta^2 = \frac{2Ea}{(2-\nu)(1+\nu)}. \quad (\text{A4})$$

Thus, η can be expressed only by the Poisson's ratio,

$$\eta = \sqrt{\frac{2 - \nu}{2(1 - \nu)}}. \quad (\text{A5})$$

Here we define the coefficient of restitution for subsequent discussion. We assume collision starts at $t = 0$ and compression and restitution periods terminate at $t = t_c$ and $t = t_f$, respectively. The coefficient of restitution is defined as

$$e_* = \frac{p_z(t_f) - p_z(t_c)}{p_z(t_c)} = -\frac{v_z(t_f)}{v_0}, \quad (\text{A6})$$

where $p_z(t)$ is the normal impulse, $v_z(t)$ is the normal velocity, and v_0 is the initial normal velocity. This leads to $p_z(t_f) = (1 + e_*)p_z(t_c)$ and $t_f = (1 + e_*)t_c$. In the later discussion, we assume that the effect of the coefficient of restitution e_* is obtained by changing the stiffness of the normal compliant element from κ to κ/e_*^2 at $t = t_c$. Thus, from eq.(A3), the normal frequency increases from Ω to Ω/e_* at $t = t_c$.

1. Normal components of velocity and Force

Now, we solve eq.(A1) and obtain normal and tangential components of velocity and force. Assuming $v_z(t) + \dot{u}_z(z) = 0$ during contact, we obtain

$$v_z(t) = \begin{cases} v_z(0) \cos \Omega t & 0 \leq t \leq t_c \\ e_* v_z(0) \cos(\frac{\Omega t}{e_*} + \frac{\pi}{2}(1 - e_*^{-1})) & t_c \leq t \leq t_f. \end{cases} \quad (\text{A7})$$

Assuming that the normal frequencies during restitution is Ω/e_* and the initial conditions $v_z(t_c) = 0$ and $v_z(t_f) = -e_*$, we reach the exact form of solution during restitution period. (A7) is continuous at $t = t_c$. By differentiating these expressions, we also obtain the displacement $u_z(t)$, the force $F_z(t)$, and the impulse $p_z(t)$ as described in Table I.

2. Tangential Components of Velocity and Force

We assume that a disk sticks or slips on the surface of a rectangle during collision and starts sticking at $t = t_2$. At $t = t_2$, the relation between F_x and F_z becomes $|F_x| < \mu F_z$. We calculate the expressions for tangential components for sticking and slipping separately.

While a disk slips on the surface of a rectangle, the relation between F_x and F_z is $|F_x|/F_z = \mu$ and the tangential velocity is changed by a impulse arising from contact force. Thus, The change of velocity can be described as

$$\begin{pmatrix} dv_x/dp_3 \\ dv_z/dp_3 \end{pmatrix} = m^{-1} \begin{bmatrix} \beta_x \eta^{-2} & 0 \\ 0 & \beta_z \end{bmatrix} \begin{pmatrix} -\mu \text{sgn}(v_x + \dot{u}_x) \\ 1 \end{pmatrix} \quad t < t_2, \quad (\text{A8})$$

where $\text{sgn}(x) = +1$ for $x > 0$ and $\text{sgn}(x) = -1$ for $x < 0$.

When a disk starts sticking at $t = t_2$, the tangential oscillation starts with frequency ω . We assume $v_x(t) + \dot{u}_x(t) = 0$. By solving the equation of $u_x(t)$, we can obtain the tangential components of displacement, velocity, and contact force as

$$\begin{aligned} u_x(t) &= u_x(t_2) \cos \omega(t - t_2) - \omega^{-1} v_x(t_2) \sin \omega(t - t_2) \\ v_x(t) &= \omega u_x(t_2) \sin \omega(t - t_2) + v_x(t_2) \cos \omega(t - t_2) \\ F_x(t) &= m \beta_x^{-1} \omega^2 u_x(t_2) \cos \omega(t - t_2) - m \beta_x^{-1} \omega v_x(t_2) \sin \omega(t - t_2) \quad t \geq t_2. \end{aligned} \quad (\text{A9})$$

3. Obtaining the transition time, t_1

We think the situation that stick begins at the initial instant contact, *i.e.* $t_2 = 0$, and slip begins at $t = t_1$. From (A9) with the condition $u_x(0) = 0$ and $F_z(t)$ described in the Table I, t_1 can be obtained solving the equation

$$\frac{|F_x(t_1)|}{\mu F_z(t_1)} = \begin{cases} \frac{1}{\eta^2} \frac{v_x(0)}{\mu v_z(0)} \frac{\Omega \sin \omega t_1}{\omega \sin \Omega t_1} = 1 & 0 \leq t_1 < t_c \\ \frac{1}{\eta^2} \frac{v_x(0)}{\mu v_z(0)} \frac{\Omega \sin \omega t_1}{\omega \sin(\frac{\Omega t_1}{e_*} + \frac{\pi}{2}(1 - e_*^{-1}))} = 1 & t_c \leq t_1 < t_f. \end{cases} \quad (\text{A10})$$

Solving these equation numerically, we obtain t_1 . It should be noted that there are two conditions if t_1 is greater or smaller than t_c .

The process of initial stick takes place if $t_1 > 0$, *i.e.* if in the limit as $t_1 \rightarrow 0$ the force ratio between the tangential and normal component is smaller than μ . This requires

$$\frac{v_x(0)}{v_z(0)} < \mu \eta^2. \quad (\text{A11})$$

4. Three Regimes of The Angle of Incidence

Here, we divide all region of the angle of incidence into three regimes and calculate the tangential component of terminal velocity of collision for each regime.

(i) **small angle of incidence:** $v_x(0)/v_z(0) < \mu\eta^2$

In this regime, initial stick continues until $t = t_1$ and slip terminates at $t = t_f$. At time t_1 , the tangential component of the relative velocity is $v_x(t_1) = v_x(0) \cos \omega t_1$. From eq.(A8), the terminal tangential velocity can be expressed as

$$v_x(t_f) = v_x(0) \cos \omega t_1 - \frac{\mu\beta_x}{m}[p_z(t_f) - p_z(t_1)], \quad (\text{A12})$$

where $p_z(t_f) - p_z(t_1)$ can be expressed as

$$p_z(t_f) - p_z(t_1) = -m \frac{v_z(0)}{\beta_z} e_* \left\{ 1 + \cos\left(\frac{\Omega t_1}{e_*} + \frac{\pi}{2}(1 - e_*^{-1})\right) \right\} \quad (\text{A13})$$

from Table I. Dividing eq.(A12) by $-v_x(0)$ leads to

$$\beta = -\cos \omega t_1(\gamma) - \mu \frac{\beta_x}{\beta_z} e \left[1 + \cos\left(\frac{\Omega t_1(\gamma)}{e} + \frac{\pi}{2}(1 - e^{-1})\right) \right] \cot \gamma, \quad (\text{A14})$$

where β is $-v_x(t_f)/v_x(0)$ and $\cot \gamma$ is $v_z(0)/v_x(0)$.

(ii) **intermediate angle of incidence:** $\mu\eta^2 < v_x(0)/v_z(0) < \mu(1 + e_*)\beta_x/\beta_z$

In this regime, the disk initially slips and begins to stick at $t = t_2$. After the period of sticking, the disk begins to slip again at $t = t_3$. In the period $t < t_2$, the tangential component of relative velocity is written as

$$v_x(t) = v_x(0) - \frac{\mu\beta_x}{m} p_z(t). \quad (\text{A15})$$

Here let us calculate t_2 and t_3 . At $t = t_2$, subsequent sliding and stick give the same rate of change for the tangential force:

$$\lim_{\epsilon \rightarrow 0} \left| \frac{dF_x(t_2 + \epsilon)}{d\epsilon} \right| = \lim_{\epsilon \rightarrow 0} \mu \frac{dF_z(t_2 + \epsilon)}{d\epsilon}. \quad (\text{A16})$$

This is the condition which determines t_2 . To simplify this condition, we need to obtain the exact forms of $dF_x(t)/dt$ and $dF_z(t)/dt$.

For tangential components of force, if one differentiate eq.(A9) by t , we obtain

$$\frac{dF_x(t)}{dt} = \frac{m\omega^3 u_x(t_2)}{\beta_x} \sin \omega(t - t_2) - \frac{m\omega^2 v_x(t_2)}{\beta_x} \cos \omega(t - t_2) \quad t > t_2. \quad (\text{A17})$$

Here, $v_x(t)$ is represented by eq.(A15) and with the aid of Table I, and $u_x(t)$ is obtained from $v_x(t) + \dot{u}_x(t) = 0$. Thus, the explicit expressions are

$$\begin{aligned} v_x(t_2) &= \begin{cases} v_x(0) - \mu \frac{\beta_x}{\beta_z} v_z(0) [1 - \cos \Omega t_2] & t_2 \leq t_c \\ v_x(0) - \mu \frac{\beta_x}{\beta_z} v_z(0) \left[1 - \cos \left(\frac{\Omega t_2}{e_*} + \frac{\pi}{2} (1 - e_*^{-1}) \right) \right] & t_2 > t_c \end{cases} \\ u_x(t_2) &= \begin{cases} \mu \frac{\beta_x \Omega v_z(0)}{\beta_z \omega^2} \sin \Omega t_2, & t_2 \leq t_c \\ \mu \frac{\beta_x \Omega v_z(0)}{\beta_z \omega^2} \sin \left(\frac{\Omega t_2}{e_*} + \frac{\pi}{2} (1 - e_*^{-1}) \right) & t_2 > t_c \end{cases} \end{aligned} \quad (\text{A18})$$

For normal components of force, by differentiating the expressions of normal components in Table I, we can obtain

$$\frac{dF_z(t_2)}{dt} = \begin{cases} -\beta_z^{-1} \Omega^2 m v_z(0) \cos \Omega t_2 & t_2 \leq t_c \\ -\frac{\Omega^2 m v_z(0)}{\beta_z e_*} \cos \left(\frac{\Omega t_2}{e_*} + \frac{\pi}{2} (1 - e_*^{-1}) \right) & t_2 \geq t_c \end{cases} \quad (\text{A19})$$

From (A17), (A18), and (A19), eq.(A16) leads to

$$\begin{aligned} \Omega t_2 &= \arccos \left(\frac{v_x(0)/\mu v_z(0) - \beta_x/\beta_z}{\eta^2 - \beta_x/\beta_z} \right) & \frac{v_x(0)}{v_z(0)} \leq \mu \frac{\beta_x}{\beta_z} \\ \frac{\Omega t_2}{e_*} &= -\frac{\pi}{2} (1 - e_*^{-1}) + \arccos \left(\frac{v_x(0)/\mu v_z(0) - \beta_x/\beta_z}{\eta^2 e_*^{-1} - e_* \beta_x/\beta_z} \right) & \frac{v_x(0)}{v_z(0)} > \mu \frac{\beta_x}{\beta_z} \end{aligned} \quad (\text{A20})$$

In the period $t_2 < t < t_3$, the velocity and the force are expressed as eq.(A9). This period of stick terminates and slip begins at time $t = t_3$. t_3 can be determined by the condition $|F_x|/F_z = \mu$. From eq.(A9) and Table I, this condition leads to

$$\left| \frac{\Omega u_x(t_2)}{\mu v_z(0)} \cos \omega(t_3 - t_2) - \frac{\Omega v_x(t_2)}{\omega \mu v_z(0)} \sin \omega(t_3 - t_2) \right| = \eta^2 \sin \left[\frac{\Omega t_3}{e_*} + \frac{\pi}{2} (1 - e_*^{-1}) \right]. \quad (\text{A21})$$

Solving this equation numerically, we obtain t_3 . The final tangential velocity is expressed as

$$v_x(t_f) = v_x(t_3) - \mu \beta_x m^{-1} [p_z(t_f) - p_z(t_3)], \quad (\text{A22})$$

where $p_z(t)$ is expressed in Table I. Dividing (A22) by $-v_x(0)$, we obtain

$$\begin{aligned} \beta &= -\cos \omega(t_3 - t_2) - \mu \frac{\beta_x}{\beta_z} [\cos \omega(t_3 - t_2) - \cos \Omega t_2 \cos \omega(t_3 - t_2)] \\ &\quad + \frac{\Omega}{\omega} \sin \Omega t_2 \sin \omega(t_3 - t_2) + e + \cos \Omega t_3 \cot \gamma. \end{aligned} \quad (\text{A23})$$

(iii) **Large angle of incidence:** $v_x(0)/v_z(0) > \mu(1 + e_*)\beta_x/\beta_z$

In this regime, slip does not cease before separation: $t_2 > t_f$. At separation, the tangential velocity $v_x(t_f)$ is as follows:

$$v_x(t_f) = v_x(0) + \mu\beta_x m^{-1}(1 + e_*)p_z(t_c), \quad (\text{A24})$$

where $p_z(t_c) = -mv_z(0)/\beta_z$. Thus, dividing (A24) by $-v_x(0)$, we obtain

$$\beta = -1 + \mu \frac{\beta_x}{\beta_z} (1 + e) \cot \gamma. \quad (\text{A25})$$

APPENDIX B: POISSON'S RATIO OF THE SQUARE LATTICE SYSTEM

In this Appendix, we derive the relation between elastic constants in continuum limit and spring constants of a two-dimensional square lattice with nearest neighbor coupling k_1 and next nearest neighbor coupling k_2 . The elastic tensor C_{ijkl} for the two dimensional square lattice is represented as

$$C_{xxxx} = C_{yyyy} = k_1 + k_2, \quad (\text{B1})$$

$$C_{xxyy} = C_{yyxx} = C_{xyyx} = C_{yxyx} = C_{xyxy} = C_{yxxy} = k_2, \quad (\text{B2})$$

and the other coefficients are zero[41].

Using the elastic tensor C_{ijkl} and the strain tensor u_{ij} and u_{kl} , The free energy of the system U is represented as

$$U = \frac{1}{2} C_{ijkl} u_{ij} u_{kl}. \quad (\text{B3})$$

Thus, we obtain the stress tensor σ_{ij} as

$$\sigma_{ij} = \frac{\partial U}{\partial u_{ij}} = C_{ijkl} u_{kl}. \quad (\text{B4})$$

Now we introduce the unit vector \mathbf{n} in the axial direction of the rod. When we pull both sides of the rod with the pressure p , the relation

$$\sigma_{ik} = p n_i n_k \quad (\text{B5})$$

holds.

From Eqs (B1), (B2) and (B5), the explicit expressions of the stress tensors become

$$\sigma_{xx} = C_{xxxx} u_{xx} + C_{xxyy} u_{yy} = (k_1 + k_2) u_{xx} + k_2 u_{yy} = p n_x^2 \quad (\text{B6})$$

$$\sigma_{yy} = C_{yyxx} u_{xx} + C_{yyyy} u_{yy} = k_2 u_{xx} + (k_1 + k_2) u_{yy} = p n_y^2 \quad (\text{B7})$$

$$\sigma_{xy} = C_{xyxy} u_{xy} + C_{xyyx} u_{yx} = 2k_2 u_{xy} = p n_x n_y. \quad (\text{B8})$$

From these equations, we obtain the expressions of the strain tensors,

$$u_{xx} = p \frac{(k_1 + k_2)n_x^2 - k_2 n_y^2}{k_1(k_1 + 2k_2)} \quad (\text{B9})$$

$$u_{yy} = p \frac{(k_1 + k_2)n_y^2 - k_2 n_x^2}{k_1(k_1 + 2k_2)} \quad (\text{B10})$$

$$u_{xy} = p \frac{n_x n_y}{2k_2}. \quad (\text{B11})$$

The strain in the direction of \mathbf{n} is expressed as $u = u_{ik}n_i n_k$. Thus, we have

$$u = u_{xx}n_x^2 + 2u_{xy}n_x n_y + u_{yy}n_y^2 \quad (\text{B12})$$

$$= \left\{ \frac{k_1 + k_2}{k_1(k_1 + 2k_2)} + \frac{k_1 - 2k_2}{k_1 k_2} n_x^2 n_y^2 \right\} p. \quad (\text{B13})$$

Therefore we obtain Young's modulus as

$$\frac{1}{E} = \frac{k_1 + k_2}{k_1(k_1 + 2k_2)} + \frac{k_1 - 2k_2}{k_1 k_2} n_x^2 n_y^2 \quad (\text{B14})$$

On the other hand, the Poisson's ratio ν is defined as the ratio of the normal strain to the vertical strain. The latter is described as

$$u_t = u_{xx}n_y^2 - 2u_{xy}n_x n_y + u_{yy}n_x^2 \quad (\text{B15})$$

$$= \left\{ \frac{2(k_1 + 2k_2)n_x^2 n_y^2 - k_2}{k_1(k_1 + 2k_2)} - \frac{n_x^2 n_y^2}{k_2} \right\} p. \quad (\text{B16})$$

Thus, Poisson's ratio is given by

$$\nu = \frac{k_2^2 + (k_1^2 - 4k_2^2)n_x^2 n_y^2}{k_2(k_1 + k_2) + (k_1^2 - 4k_2^2)n_x^2 n_y^2}. \quad (\text{B17})$$

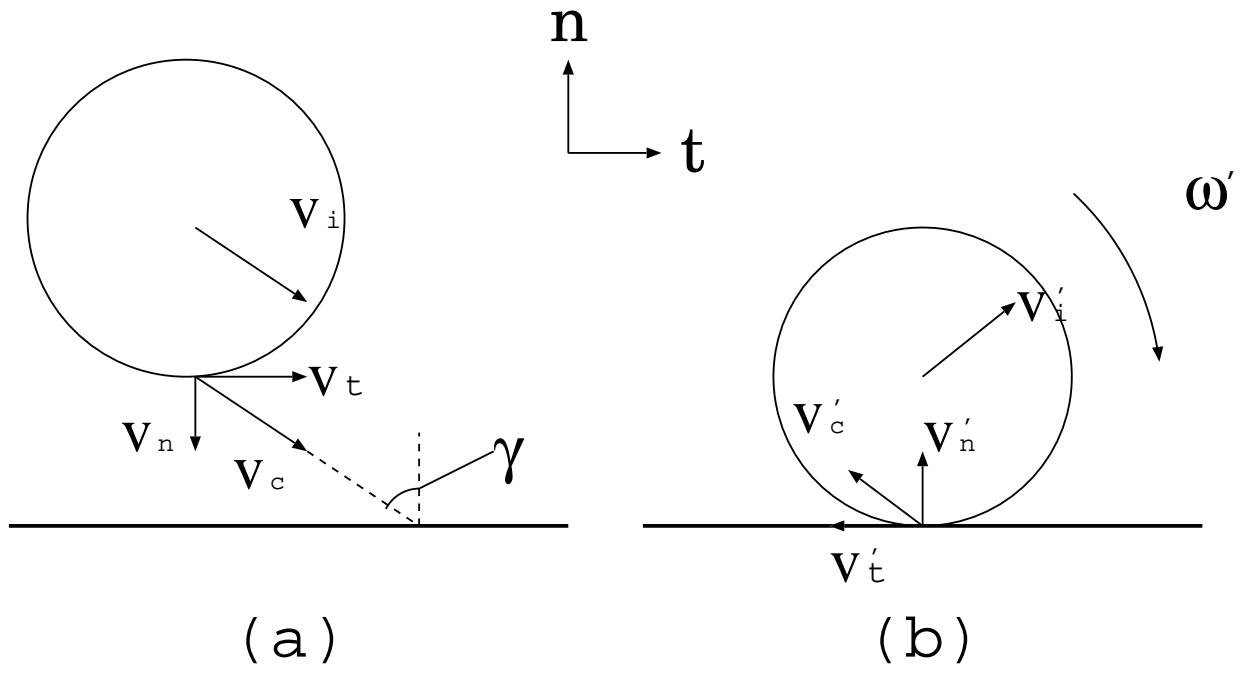


FIG. 1: H. Kuninaka and H. Hayakawa

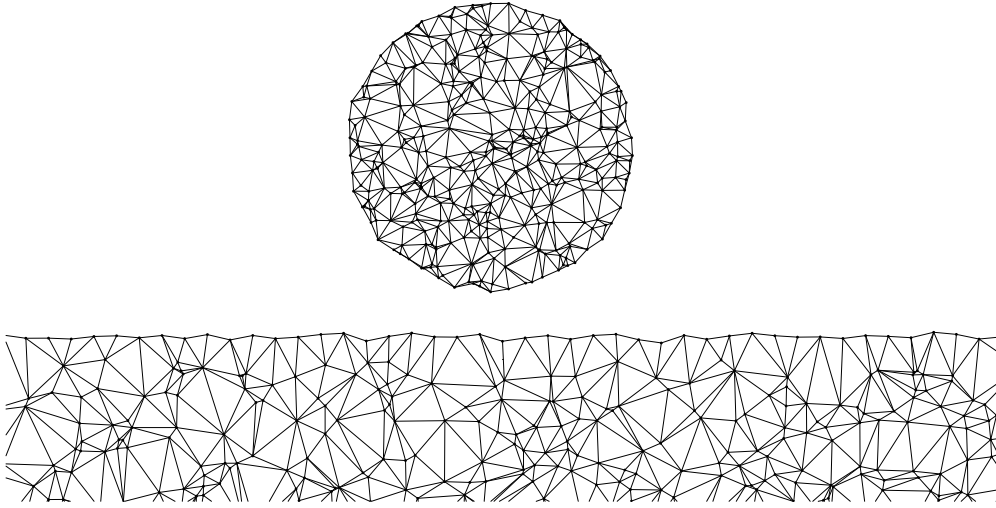


FIG. 2: H. Kuninaka and H. Hayakawa

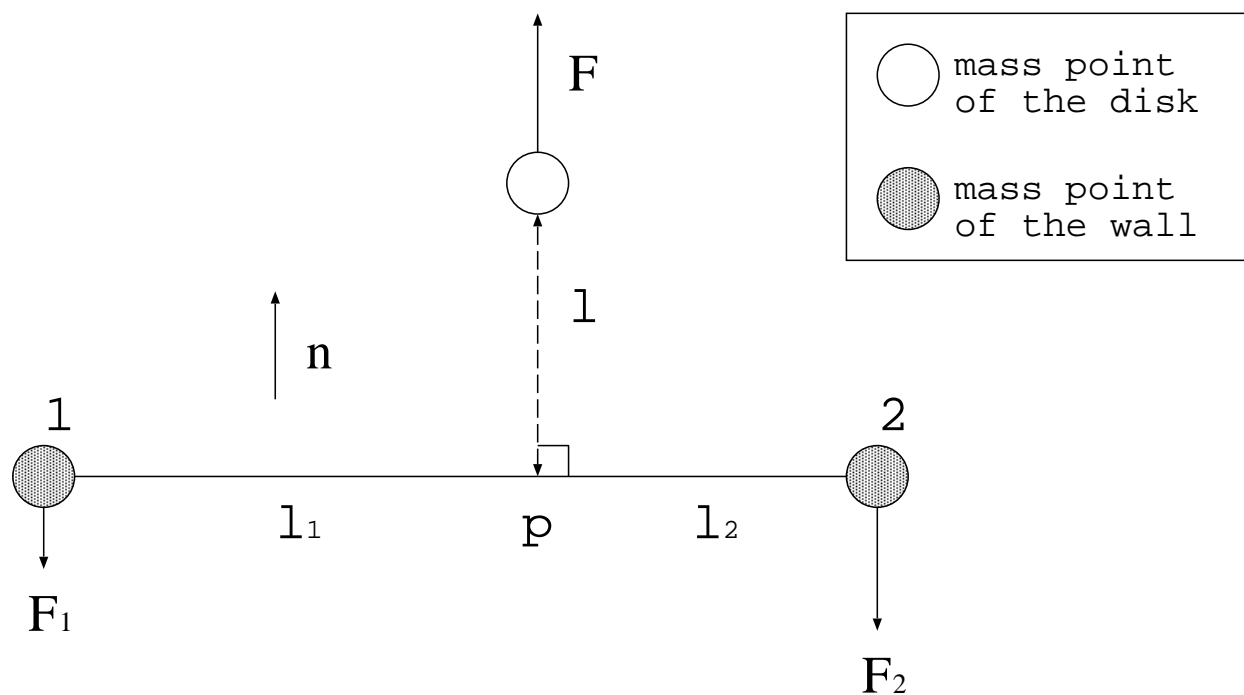
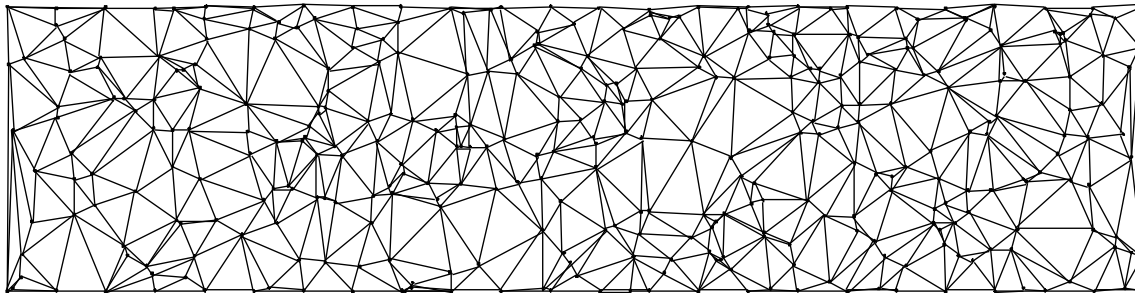
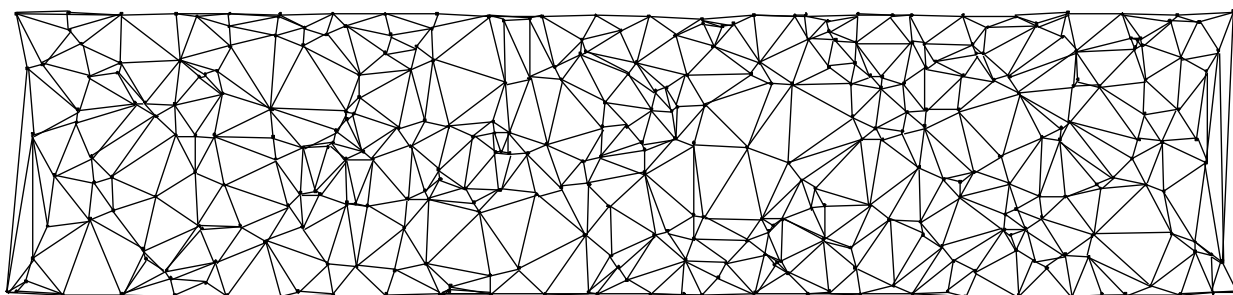


FIG. 3: H. Kuninaka and H. Hayakawa

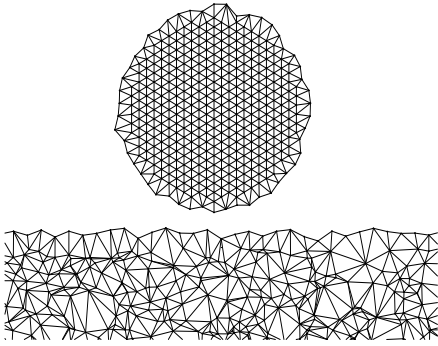


(a)

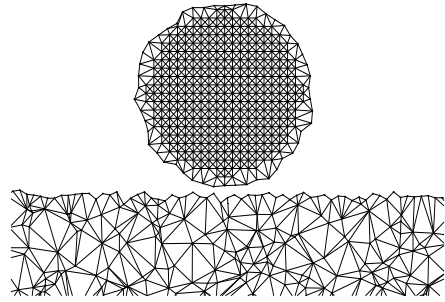


(b)

FIG. 4: H. Kuninaka and H. Hayakawa



(a)



(b)

FIG. 5: H. Kuninaka and H. Hayakawa

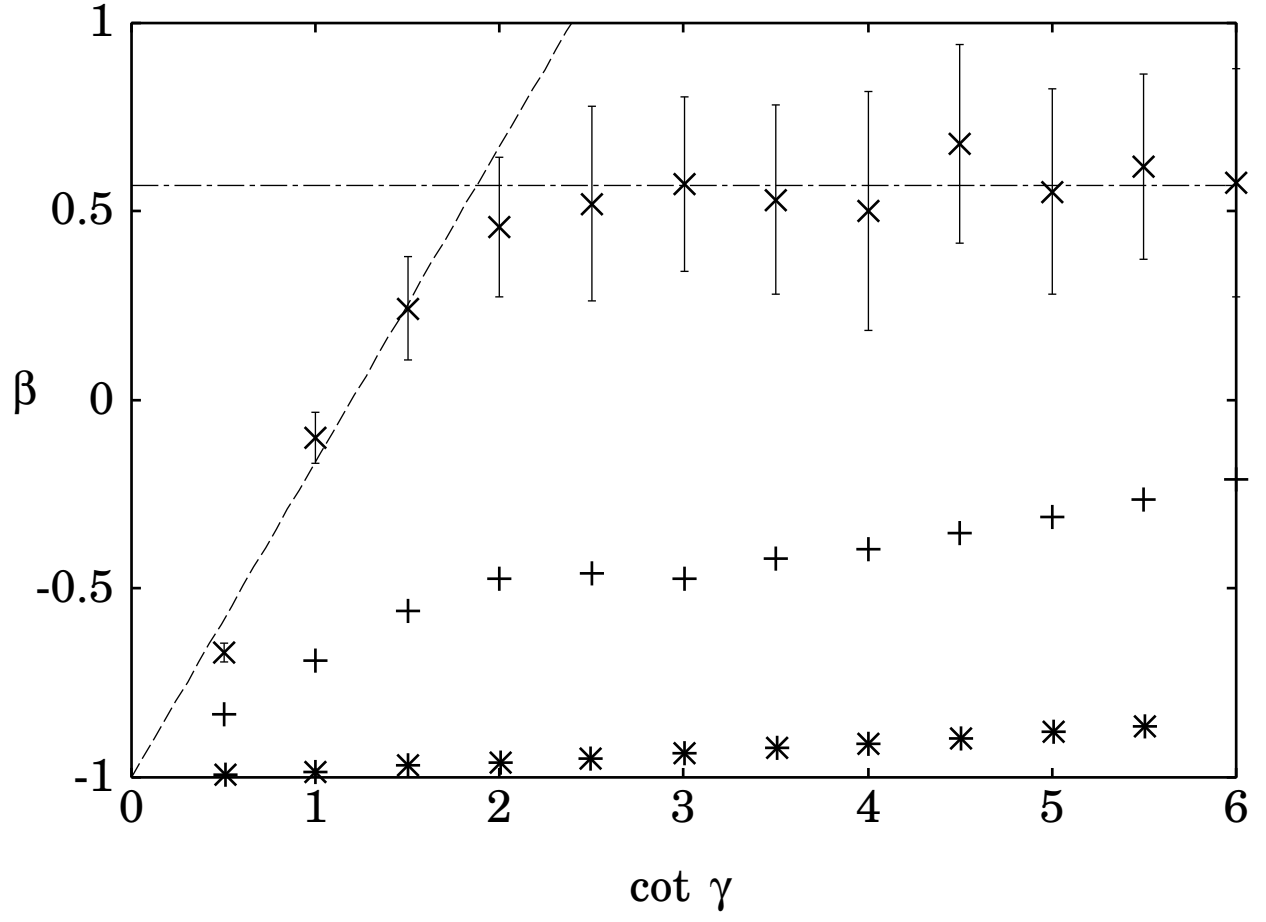


FIG. 6: H. Kuninaka and H. Hayakawa

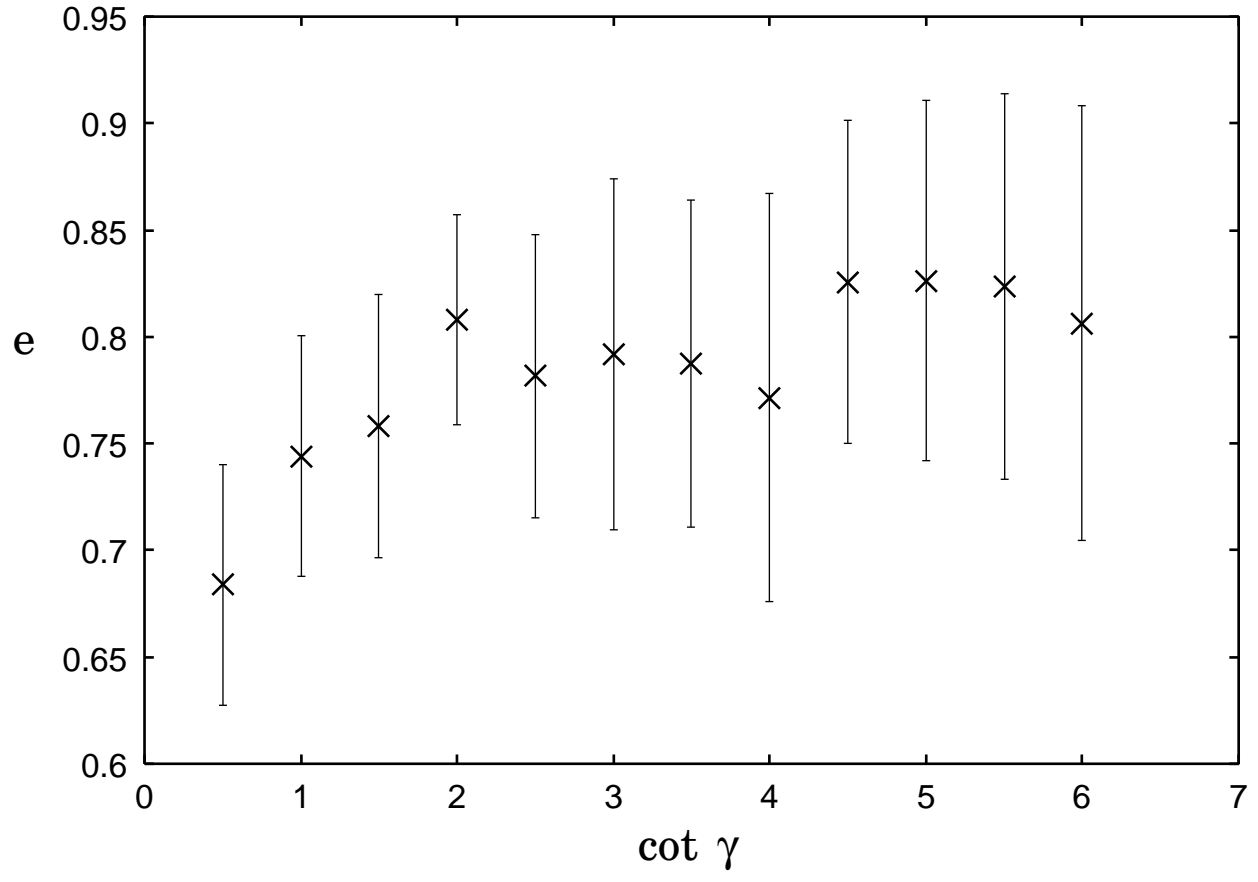


FIG. 7: H. Kuninaka and H. Hayakawa

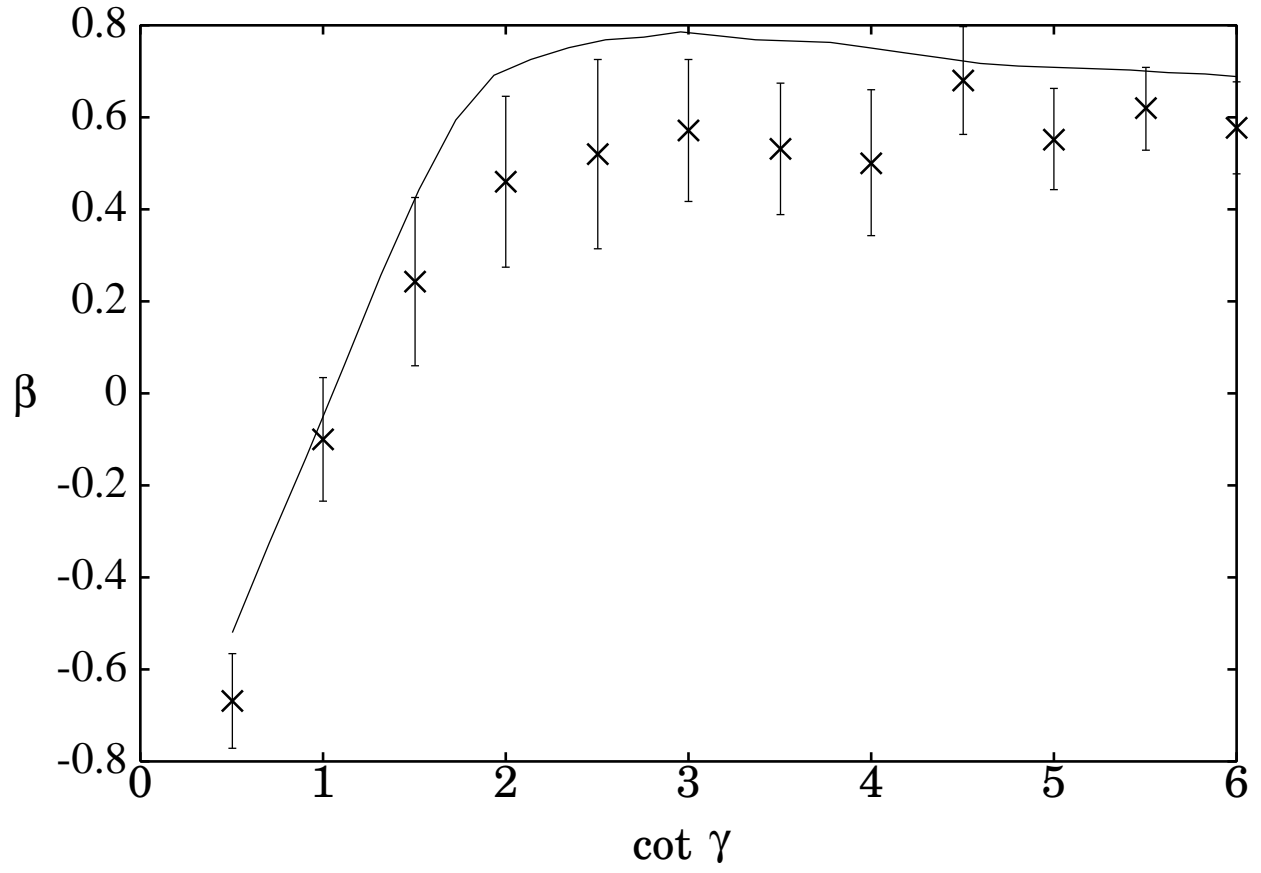


FIG. 8: H. Kuninaka and H. Hayakawa

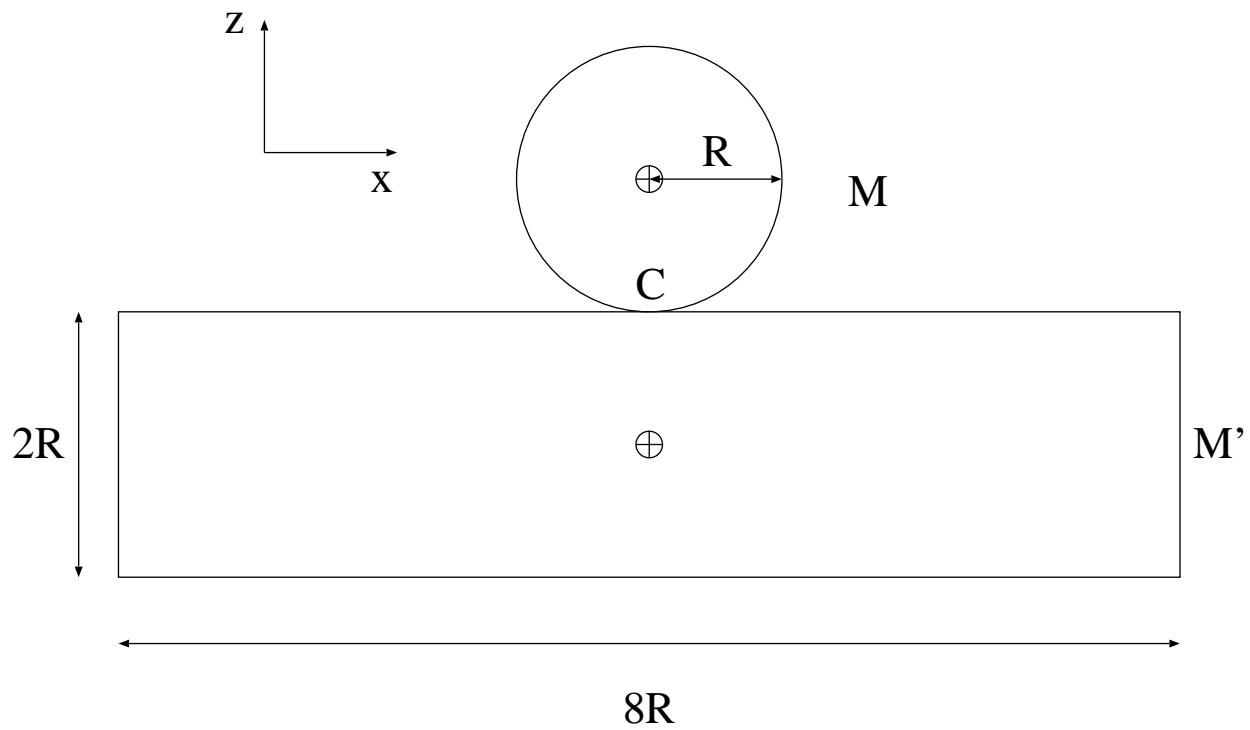


FIG. 9: H.Kuninaka and H. Hayakawa

TABLE I: Normal displacement, velocity, force, and impulse

Quantity	Compression ($0 \leq t \leq t_c$)	Restitution ($t_c \leq t \leq t_f$)
Displacement	$u_z(t) = -\Omega^{-1}v_z(0) \sin \Omega t$	$u_z(t) = -e_*^2 \Omega^{-1}v_z(0) \sin \left(\frac{\Omega t}{e_*} + \frac{\pi}{2} (1 - e_*^{-1}) \right)$
Velocity	$v_z(t) = v_z(0) \cos \Omega t$	$v_z(t) = e_*^2 v_z(0) \cos \left(\frac{\Omega t}{e_*} + \frac{\pi}{2} (1 - e_*^{-1}) \right)$
Force	$F_z(t) = -\frac{m\Omega v_z(0)}{\beta_z} \sin \Omega t \geq 0$	$F_z(t) = -\frac{m\Omega v_z(0)}{\beta_z} \sin \left(\frac{\Omega t}{e_*} + \frac{\pi}{2} (1 - e_*^{-1}) \right) \geq 0$
Impulse	$p_z(t) = -\frac{mv_z(0)}{\beta_z} (1 - \cos \Omega t)$	$p_z(t) = -\frac{mv_z(0)}{\beta_z} \left(1 - e_* \cos \left(\frac{\Omega t}{e_*} + \frac{\pi}{2} (1 - e_*^{-1}) \right) \right)$